Short Papers

Preview Control of Dual-Stage Actuator Systems for Superfast Transition Time

Aurélio T. Salton, Zhiyong Chen, Jinchuan Zheng, and Minyue Fu

***Abstract*—This paper introduces a preview control design method to reduce the settling time of dual-stage actuators (DSAs). A DSA system is comprised of two actuators connected in series, a primary (coarse) actuator, and a secondary (fine) actuator. The objective of the proposed design is to account for the redundancy of actuators and use the information of future reference levels in order to compute a pair of inputs to be applied before the output transition time. Experimental results show that the proposed design method significantly reduces the output transition time when compared to conventional forms of DSA control design.**

***Index Terms*—Dual-stage actuator (DSA), motion control, nonlinear feedback, preview control.**

I. Introduction

In this paper, we address the issue of reducing the output transition time interval of dual-stage actuators (DSAs) from an initial reference $\text{ref}(t \leq \tau) = \text{ref}_i$ to a final reference $\text{ref}(t > \tau) = \text{ref}_{i+1}$. The proposed approach makes use of the information on future reference levels in order to compute a pair of inputs to be applied before the transition instant $(t = \tau)$. The developed preview control strategy is suitable for any system that accounts with redundant actuators and prior knowledge of future reference points, and is particularly, interesting for systems facing the successive setpoint scenario.

The problem of settling time reduction of single-stage actuator systems has been thoroughly studied in the past few decades. In particular, two of the most important achievements in the area are the proximate time-optimal servomechanism (PTOS) by Workman [1], and the composite nonlinear feedback (CNF) by Lin *et al.* [2]. In more recent years, an effort to extend these results to DSA has been made, Peng *et al.* has adapted CNF for DSA hard-disk drives (HDDs) [3], Herrmann *et al.* has developed a robust antiwindup scheme to deal with the saturation of the secondary actuator, while applying the PTOS to the primary [4], and Zheng and Fu integrated both the PTOS and the CNF for DSA in [5]. However, there are very few works that deal with preview control or preactuation of DSA. Most notably, one may refer to the work of Iamratanakul *et al.*, which does allow preactuation and minimizes the energy [6] and time/energy [7] during the output transition. Nonetheless, none of this work is solely dedicated to the minimization of time taking into account the saturation level of the actuators and the possibility of preactuation. In this context, we introduce the main contribution of this paper: the development of a preactuation strategy that takes into account the saturation level of the actuators and reduces the settling time of the system. Moreover, the proposed preview control methodology is fully compatible with the nonlinear state-of-art DSA design proposed in [5]. In fact, a continuous switching between both controllers is achieved for the primary actuator.

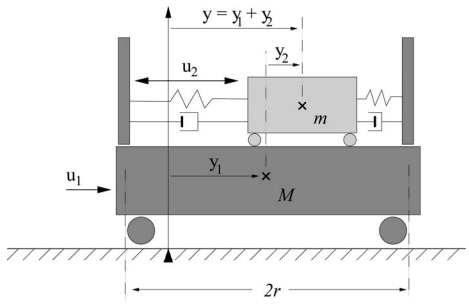

Fig. 1. Schematic representation of a DSA.

The class of systems to be considered are DSAs, such as dual-stage HDDs [8]–[10]. These systems are defined as two actuators connected in series, a primary (slow) actuator, responsible for providing the system with a long range, and a secondary (fast) actuator, responsible for improving the accuracy and speed of the system. As depicted in Fig. 1, the primary actuator is modeled as a rigid body of mass M and it is assumed that the friction acting on this actuator (if any) is actively compensated [11]. The secondary actuator is treated as a body of mass m connected in series with the primary via a spring, with spring constant k, and a damper, with damping coefficient c [12], it has a range of actuation bounded by $\pm r$ $(r > 0)$. Typically, DSA's have the features that $M \gg m$ and $|u_2/u_1| \gg m/(M+m)$, which allows us to neglect the coupling forces between the primary and the secondary actuators. In this way, the DSA of interest is modeled as a linear decoupled dual-input single-output (DISO) system, which is represented in a state-space form as follows:

$$\begin{aligned} \Sigma_1 &: \dot{x}_1 = A_1 x_1 + B_1 u_1,\ x_1(0) = 0,\ |u_1| \leq \bar{u}_1 \\ \Sigma_2 &: \dot{x}_2 = A_2 x_2 + B_2 u_2,\ x_2(0) = 0,\ |u_2| \leq \bar{u}_2 \\ & y = y_1 + y_2 = C_1 x_1 + C_2 x_2 \end{aligned} \tag{1}$$

where $x_1 = [y_1 \ \ \dot{y}_1]^{\mathrm{T}}$ is associated with the primary (coarse) actuator and $x_2 = [y_2 \ \ \dot{y}_2]^{\mathrm{T}}$ with the secondary (fine) actuator, and $\bar{u}_i$ is the control saturation level for u_i. Furthermore,

$$A_1 = \begin{bmatrix} 0 & 1 \\ 0 & 0 \end{bmatrix}, B_1 = \begin{bmatrix} 0 \\ b_1 \end{bmatrix}, C_1 = [1 \quad 0]$$

$$A_2 = \begin{bmatrix} 0 & 1 \\ a_1 & a_2 \end{bmatrix}, B_2 = \begin{bmatrix} 0 \\ b_2 \end{bmatrix}, C_2 = [1 \quad 0]$$

with $a_1 = -k/m$, $a_2 = -c/m$, $b_1 = 1/(M+m)$, and $b_2 = 1/m$.

If full-state measurement is unavailable, we assume a state observer is used to estimate the unmeasured states. From the separation principle, it is well known that the complete DSA system is stable if the control laws u_1 and u_2, which are obtained assuming actual state feedback, and the state estimator are stable [13]. Therefore, we will present the

Manuscript received November 4, 2009; revised March 24, 2010 and June 2, 2010; accepted June 12, 2010. Date of publication July 23, 2010; date of current version May 11, 2011. Recommended by Technical Editor J. Xu. This work was supported by the Australian Research Councils Center of Excellence for Complex Dynamic Systems and Control.

The authors are with the School of Electrical Engineering and Computer Science, The University of Newcastle, Callaghan, NSW 2308, Australia (e-mail: aurelio.salton@uon.edu.au; zhiyong.chen@newcastle.edu.au; jinchuan.zheng@newcastle.edu.au; minyue.fu@newcastle.edu.au).

Color versions of one or more of the figures in this paper are available online at http://ieeexplore.ieee.org.

Digital Object Identifier 10.1109/TMECH.2010.2053851

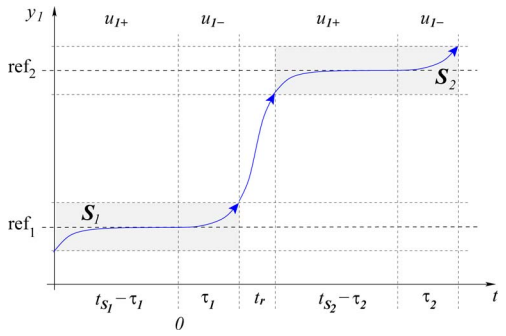

Fig. 2. Illustrative representation of the preview control strategy: t_{S_i} represents the total time the output y must stay at $\boldsymbol{S}_i$, $i = 1,\ 2$, t_r is the transition time, τ_i is the preview control time, and u_{1+} and u_{1-} differentiate between preactuation and postactuation, respectively.

rest of the paper assuming the true states are available, however, the estimated states are used during the implementation of the controllers.

II. Problem Formulation

An intrinsic characteristic of DSA systems is that the comprising actuators are complementary to each other, while the primary actuator is slow and has a large travel range, the secondary actuator is fast, but has a limited range of actuation. Due to these complementary characteristics of the DSA, it will be assumed that within the travel range of the secondary actuator, the tracking error of the primary actuator is sufficiently smooth such that it may be compensated by the secondary with negligible error.

In other words, if we define a manifold $\boldsymbol{S}_i$

$$\boldsymbol{S}_i = \{y_1 \in \mathbb{R} \ : \ |y_1 - \text{ref}_i| \le r\} \tag{2}$$

where ref_i is the ith reference level and $\pm r$ is the range of the secondary actuator, then, whenever y_1 is within the manifold $\boldsymbol{S}_i$, the total output of the system y will be at the ith reference level with negligible error. Moreover, if the output y must stay at an initial reference level ref_1 for t_S seconds before moving to another given reference ref_2, then y_1 must stay in $\boldsymbol{S}_1$ for t_S seconds before moving to $\boldsymbol{S}_2$ (see Fig. 2). We will explore this liberty of movement of the primary actuator and will allow it to move ahead of time toward the next reference. In fact, there will be a demand difference between the actuators, while the primary is being driven to ref_2 and the secondary is still tracking ref_1. Notice that it is the mechanical structure of the DSA system that allows the actuators to fulfill these different demands.

Hence, the DSA control problems may be formulated as follows:

P1: For a given initial condition $x_1(0) = [\text{ref}_1\ 0]^{\text{T}}$, two manifolds $\boldsymbol{S}_1$ and $\boldsymbol{S}_2$ determined by (2), and a control saturation level $\bar{u}_1$, find a controller

$$|u_1(t)| \le \bar{u}_1, \quad t \ge 0 \tag{3}$$

and a preview control time $\tau \ge 0$, such that the output y_1 of the primary actuator is driven from $\boldsymbol{S}_1$ to $\boldsymbol{S}_2$ with a reduced transition time t_r, in the following sense:

$$y_1(t) \in \boldsymbol{S}_1,\ 0 \le t \le \tau \tag{4}$$

$$y_1(t) \in \boldsymbol{S}_2,\ t \ge \tau + t_r, \text{ and } \lim_{t\to\infty} y_1(t) = \text{ref}_2. \tag{5}$$

P2: For a control saturation level $\bar{u}_2$, find a controller

$$|u_2(t)| \le \bar{u}_2, \quad t \ge 0 \tag{6}$$

for the secondary actuator to compensate for the error generated by the primary actuator, i.e., to achieve $y = y_1 + y_2 = \text{ref}_i$ when $y_1 \in \boldsymbol{S}_i$.

Remark 2.1: Notice that if we choose $\tau = 0$, we fall in the conventional control strategy for DSA, where no preview control is applied. Conversely, there must be an upper bound in the preview control time inasmuch as $t_S - \tau$ must be long enough, such that the primary actuator can be driven sufficiently close to the reference before any preactuation is applied.

III. Preview Control Design

A. Primary Actuator—Solvability of P1

In the literature, e.g., [14], the well-known PTOS control is largely applied to the primary actuator. This is a near time-optimal control strategy that can accommodate plant uncertainty, measurement noise, and actuator saturation. The control law is given by

$$u(t) = \text{sat}[k_2(f(e) - v_1)]$$

where $v_1 := \dot{y}_1$ and $f(e)$ is the nonnegative continuous function

$$f(e) = \begin{cases} \dfrac{k_1}{k_2}e, & \text{for } |e| \le y_l \\ \text{sgn}(e)\left(\sqrt{2b\alpha\bar{u}|e|} - \dfrac{\bar{u}}{k_2}\right), & \text{for } |e| > y_l \end{cases} \tag{7}$$

with $e := y_r - y_1$, $\boldsymbol{\alpha}$ $(0 < \boldsymbol{\alpha} < 1)$ the so-called "acceleration discount factor," and k_1 and k_2 are positive constants. In order to guarantee the continuity of the functions $f(e)$ and $f'(e)$, the following constraints are necessary [1]:

$$\boldsymbol{\alpha} = \frac{2k_1}{bk_2^2} \quad y_l = \frac{\bar{u}}{k_1}. \tag{8}$$

For the need of this paper, the role of the PTOS (7) can be summarized as follows.

Lemma 3.1: For given parameters τ, $y_1(\tau)$, $v_1(\tau)$, ref_2, and $\boldsymbol{S}_2$ determined by (2), the controller (7) with $t \in [\tau, \infty)$ drives the primary actuator from $x_1(\tau) = [y_1(\tau)\ v_1(\tau)]^{\text{T}}$ into $\boldsymbol{S}_2$ in the sense of (5). In particular, the transition time t_r is called PTOS-optimized w.r.t. $(\text{ref}_2 - y_1(\tau), v_1(\tau))$.

Clearly, for a given system and a given PTOS controller, the transition time t_r depends on the initial velocity $v_1(\tau)$ and the initial step level $\text{ref}_2 - y_1(\tau)$. Without loss of generality, we assume $\text{ref}_2 > \text{ref}_1$. Roughly speaking, t_r is reduced if $v_1(\tau)$ is larger and $\text{ref}_2 - y_1(\tau)$ is smaller. In a conventional control design, the PTOS controller applies with $v_1(\tau) = 0$ and $y_1(\tau) = \text{ref}_1$. In other words, t_r is PTOS-optimized w.r.t. $(\text{ref}_2 - \text{ref}_1,\ 0)$. Theorem 3.1 introduces a preview controller for the primary actuator, such that t_r is PTOS-optimized w.r.t. $(v_1(\tau),\ \text{ref}_2 - \text{ref}_1 - r)$ for some $v_1(\tau) > 0$.

Theorem 3.1: For any given $r > 0$, ref_i and $\boldsymbol{S}_i$ determined by (2), $i = 1, 2$; let $\delta := \text{ref}_2 - \text{ref}_1$, $\sigma = \text{sgn}(\delta)$, and $\xi = \delta - \sigma r$, and assume $|\delta| \ge 2r$. Consider the primary actuator with the initial condition $x_1(0) = [\text{ref}_1\ \ 0]^{\text{T}}$ and the controller

$$u_1 = \begin{cases} at, & 0 \le t \le \tau \\ \text{sat}[k_2(f(e) - v_1)], & t > \tau \end{cases} \tag{9}$$

with $a = 6\sigma r/(b_1\tau^3)$ and $f(e)$ from the PTOS. Then,

i) controller (9) drives the primary actuator from $\boldsymbol{S}_1$ to $\boldsymbol{S}_2$ in the sense of (5) and the output transition time is PTOS-optimized w.r.t. $(\xi,\ v_1(\tau))$ for any $\tau > 0$.
ii) in (i), if

$$\tau v_1(\tau) = 3\sigma r,\ v_1(\tau) = \sigma\sqrt{\rho\text{sat}\left(\frac{\bar{v}_\tau^2}{\rho}\right)} \tag{10}$$

where

$$\bar{v}_\tau = \sqrt{\left(\frac{\rho k_2}{2}\right)^2 + \rho k_2 f(\xi)} - \frac{\rho k_2}{2}, \quad \rho = \frac{3b_1 r}{2}$$

the controller (9) is continuous over $[0, \infty)$ and the constraints (3) and (4) are satisfied. Thus, the problem P1 is solved.

Proof: (i) During the time interval $[0, \tau)$

$$y_1(t) = b_1 \frac{a\, t^3}{6} + \text{ref}_1. \tag{11}$$

For $t = \tau$ and a given by (9), it is clear that $y_1(\tau) = \sigma r + \text{ref}_1$, which shows that the primary actuator is driven by the controller from $x_1(0) = [\text{ref}_1 \ 0]^{\mathrm{T}}$ to $x_1(\tau) = [(\text{ref}_1 + \sigma r) \ \ v_1(\tau)]^{\mathrm{T}}$. During $[\tau, \infty)$, the initial velocity for the PTOS controller (7) is $v_1(\tau)$ and the initial step level is ξ. Obviously, the transition time t_r is PTOS-optimized w.r.t. $(\xi, \ v_1(\tau))$ by Lemma 3.1.

(ii) Let τ^+ denote the right-hand limit as t tends to τ. To show that

$$u_1(\tau) = a\tau = \text{sat}(k_2(f(\xi) - v_1(\tau))) = u_1(\tau^+) \tag{12}$$

we consider two cases.

(a) *If $|\xi|$ and hence $f(\xi)$ is large, such that $\bar{v}_\tau^2 \geq \rho \bar{u}_1$.* From the second equation of (10), we have $v_1(\tau) = \sigma\sqrt{\rho \bar{u}_1}$. As a result, (12) gives on the one hand

$$u_1(\tau) = \sigma \bar{u}_1$$

and, on the other hand, (12) gives

$$u_1(\tau^+) = \text{sat}(k_2(f(\xi) - \sigma\sqrt{\rho \bar{u}_1})).$$

In this case, it suffices to show

$$k_2(f(\xi) - \sigma\sqrt{\rho \bar{u}_1}) \geq \bar{u}_1 \tag{13}$$

to prove $u_1(\tau^+) = u_1(\tau) = \sigma \bar{u}_1$. Indeed, $\bar{v}_\tau \geq \sqrt{\rho \bar{u}_1}$ gives

$$\sqrt{\left(\frac{\rho k_2}{2}\right)^2 + \rho k_2 f(\xi)} \geq \frac{\rho k_2}{2} + \sigma\sqrt{\rho \bar{u}_1}$$

by squaring both sides

$$k_2 f(\xi) \geq k_2 \sigma \sqrt{\rho \bar{u}_1} + \bar{u}_1$$

and hence (13).

(b) *If $|\xi|$ and hence $f(\xi)$ is small, such that $\bar{v}_\tau^2 < \rho \bar{u}_1$.* From the second equation of (10), we have $v_1(\tau) = \sigma \bar{v}_\tau$. Then, (12) gives $u_1(\tau) = \sigma \bar{v}_\tau^2 / \rho$, and

$$u_1(\tau^+) = \text{sat}(k_2(f(\xi) - v_1(\tau))).$$

It suffices to show

$$k_2(f(\xi) - v_1(\tau)) = \frac{\bar{v}_\tau^2}{\rho} < \bar{u}_1$$

to prove $u_1(\tau^+) = u_1(\tau)$. Indeed, the equation holds from the definition of $\bar{v}_\tau$ and the inequality from the assumption directly. From aforementioned expression, we have proven $u_1(0) = 0$ and $u_1(\tau) = u_1(\tau^+)$, i.e., the controller (9) is continuous over $[0, \infty)$.

Next, notice that the preview control law is monotonic and $v_1(0) = 0$, then y_1 moves from $y_1(0) = \text{ref}_1$ to $y_1(\tau) = \text{ref}_1 + \sigma r$ monotonically. Therefore, the constraint (4) is satisfied.

Finally, by noting $v_1(\tau)^2 \leq \rho \bar{u}_1$ from the second equation of (10), for $0 \leq t \leq \tau$, we have

$$|u_1(t)| = |at| \leq |a\tau| = \frac{v_1(\tau)^2}{\rho} \leq \bar{u}_1$$

which proves the constraint (3). The proof is thus complete. □

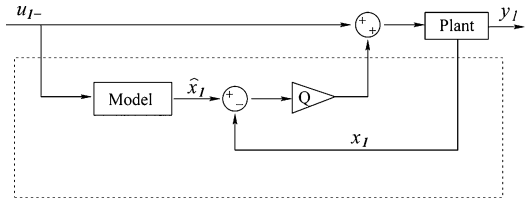

Fig. 3. Preview control strategy implemented through a feedforward/feedback scheme during preactuation (represented by u_{1-}) in order to add robustness to the controller.

In Theorem 3.1, we assume $|\delta| \geq 2r$ (or, $|\xi| \geq r$), which means that the two manifold $\boldsymbol{S}_1$ and $\boldsymbol{S}_2$ do not overlap. When $|\delta| < 2r$ (or, $|\xi| < r$), the controller in Theorem 3.1 may not work directly because a small $|\xi|$ gives a small $f(\xi)$, and hence, a small $v_1(\tau)$, which implies a large τ. In particular, when $|\delta| = r$, we have $\xi = 0$ and $\tau = \infty$. However, τ should be small enough, such that $t_S - \tau$ is sufficient for the previous PTOS to settle down. Nevertheless, the controller in Theorem 3.1 still works with a slight modification by resetting a smaller $r = |\delta|/2$. With this modification, we will show that there is an upper boundary for τ, which is independent of r, ref_1, and ref_2. The result is given as following.

Corollary 3.1: For a given $\bar{r}$ and any $r \in (0, \bar{r}]$, the preview control time τ set in Theorem 3.1(ii) has an upper boundary, i.e., $\tau \leq \bar{\tau}$, where $\bar{\tau}$ is independent of r, ref_1, and ref_2. In particular,

$$\bar{\tau} = 3/\min\{\sqrt{\bar{\rho}\bar{u}_1/\bar{r}}, \ \ \sqrt{(\bar{\rho}k_2/2)^2 + \bar{\rho}\bar{k}_1} - \bar{\rho}k_2/2\}$$
$$\bar{\rho} = (3b_1)/2, \ \bar{k}_1 = \min\{k_1, \bar{u}_1/\bar{r}\}.$$

Proof: In Theorem 3.1, we assume $|\delta| \geq 2r$, which implies $|\xi| \geq r$. From the definitions of f and $\bar{k}_1$, we have

$$\frac{f(\xi)}{r} \geq \frac{f(r)}{r} \geq \bar{k}_1. \tag{14}$$

Since (10) give $\tau = 3\sigma r / v_1(\tau)$, with $\bar{\rho} = \rho / r$, we have $\tau = 3/\sqrt{(\bar{\rho}/r)\text{sat}(\bar{v}_\tau^2/(\bar{\rho}r))}$, and it suffices to prove

$$\sqrt{(\bar{\rho}/r)\text{sat}(\bar{v}_\tau^2/(\bar{\rho}r))} \geq \min\{\sqrt{\bar{\rho}\bar{u}_1/\bar{r}}, \ \ \sqrt{(\bar{\rho}k_2/2)^2 + \bar{\rho}\bar{k}_1} - \bar{\rho}k_2/2\}. \tag{15}$$

If $\bar{v}_\tau^2/(\bar{\rho}r) \geq \bar{u}_1$, the inequality (15) holds obviously. Otherwise, we have

$$\text{lhs} = \bar{v}_\tau / r = \sqrt{(\bar{\rho}k_2/2)^2 + \bar{\rho}f(\xi)/r} - \bar{\rho}k_2/2 \geq \text{rhs}$$

using (14). The proof is thus complete. □

Remark 3.1: In order to add robustness to the preview control strategy, the feedback/feedforward scheme in Fig. 3 may be implemented. The preview control input is applied to an internal reference model, from which the desired trajectory $\hat{x}_1$ is obtained. Then, this trajectory is tracked by applying the designed preview input as a feedforward reference and by stabilizing the system with a linear feedback gain $Q = [q_1 \ q_2]$, which may be computed by classical linear control techniques.

B. Secondary Actuator—Solvability of P2

The secondary actuator controller is a form of CNF borrowed from [5]. Its control law is given by

$$u_2 = \text{sat}(u_{2L} + u_{2N}) \tag{16}$$

where u_{2L} is a linear feedback law, which stabilizes the secondary actuator with a higher bandwidth than that of the primary, and u_{2N} is a nonlinear feedback law, which improves the performance of the overall DSA system. The linear controller is given by standard-state-feedback gain

$$u_{2L} = Wx_2 \tag{17}$$

where $W = [w_1 \ w_2]$ may be calculated by any linear control technique. The nonlinear feedback controller is given by

$$u_{2N} = \gamma(\mathrm{ref}_2, y)H \begin{bmatrix} y_1 - \mathrm{ref}_2 \\ v_1 \end{bmatrix} \tag{18}$$

where H is chosen as follows:

$$H = \frac{1}{b_2}\left[(a_1 + b_2 w_1 + b_1 k_1) \quad (a_2 + b_2 w_2 + b_1 k_2)\right] \tag{19}$$

with constants k_1 and k_2 from (7), and the nonlinear function $\gamma(\cdot)$ is as follows:

$$\gamma(\mathrm{ref}_2, y) = e^{-\beta|\mathrm{ref}_2 - y|} \tag{20}$$

and β is a tuning parameter.

Due to the proper choice of H and $\gamma(\mathrm{ref}_2, y)$, the DSA closed-loop dynamics change from the primary to the secondary actuator control loop as the system approaches the reference level. This transition results in an improved performance, inasmuch as the secondary actuator is designed to have a high bandwidth and a small damping ratio, allowing it to compensate the overshoot generated by the primary actuator [5]. Therefore, for the DSA system in (1) with the primary actuator under the control law (9), the secondary actuator under the nonlinear control law (16) is able to compensate for the error generated by the primary actuator. Moreover, constraint (6) is satisfied as long as the primary actuator remains in $\boldsymbol{S}_i$, which is guaranteed by the preview control formulation. Thus, problem P2 is solved.

IV. Experimental Results

The advantages obtained with the proposed control scheme are demonstrated with an experimental setup [5] comprised of a linear motor (LM) as the primary stage and a piezoactuator (PZT) as the secondary stage. The LM has a 0.5-m travel range and a 1-μm resolution glass scale encoder. The PZT has a maximum travel range of ± 15 μm and an integrated capacitive position sensor with 0.2 nm resolution to measure the relative displacement between the LM and the PZT. For this particular system, $\overline{u}_1 = 1$ V and $\overline{u}_2 = 5$ V, and the parameters a_1, a_2, b_1, and b_2 were identified experimentally and are given by

$$\begin{aligned} a_1 &= -10^6, \quad b_1 = 1.5 \times 10^7 \\ a_2 &= -1810, \quad b_2 = 3 \times 10^6. \end{aligned} \tag{21}$$

When working in its linear region, the PTOS control law becomes a linear feedback gain $K = [k_1 \ k_2]$, which may be parameterized as follows:

$$K = \frac{1}{b_1}[(2\pi\omega_1)^2 \quad 4\pi\omega_1\zeta_1] \tag{22}$$

with ω_1 and ζ_1 are the natural frequency and damping ratio of the primary actuator closed-loop system. By pushing $\omega_1 = 30$ Hz, the PTOS linear region is given by $|\mathrm{ref}_2 - p(t)| \leq 422$ μm. Similarly, the PZT gain is calculated by choosing $\omega_2 = 300$ Hz. The gains are given by

$$\begin{aligned} K &= 10^{-3} \times [2.4 \ \ 0.0225] \\ W &= -[0.8385 \ \ 0.0005] \\ H &= -[1.1602 \ \ 0.001] \end{aligned} \tag{23}$$

and for the nonlinear function (20), the free parameter is chosen as $\beta = 0.001$. Finally, when implementing the preview control law, given ref_2 and according to (10), one must first compute the final velocity $v_1(\tau)$ followed by the preview control time τ, the control law (9) is then applied via the feedback/feedforward scheme, as shown in Fig. 3.

Three forms of DSA control strategy were compared in the experimental setup: 1) the dual-stage servo design proposed in [15], where CNF is applied to primary actuator; 2) the nonlinear feedback control without preactuation, where the primary actuator is tuned to present some overshoot for improved performance [5]; and 3) the proposed preview control strategy. All controllers were implemented by a DSP system (dSPACE-DS1103) with the sampling frequency of 5 kHz, and settling time was defined as the time it takes for the total position output y to enter and remain within ± 2 μm relative to the setpoint.

Fig. 4 shows the system response to a 15-μm step reference, which is within the range of the secondary actuator. Notice that this response is dominated by the dynamics of the secondary and there is little difference between the performance of the comparative controllers. Nevertheless, as shown in Fig. 4, the proposed method is still able to achieve some improvement over controllers (a) and (b) when seeking the 15-μm reference.

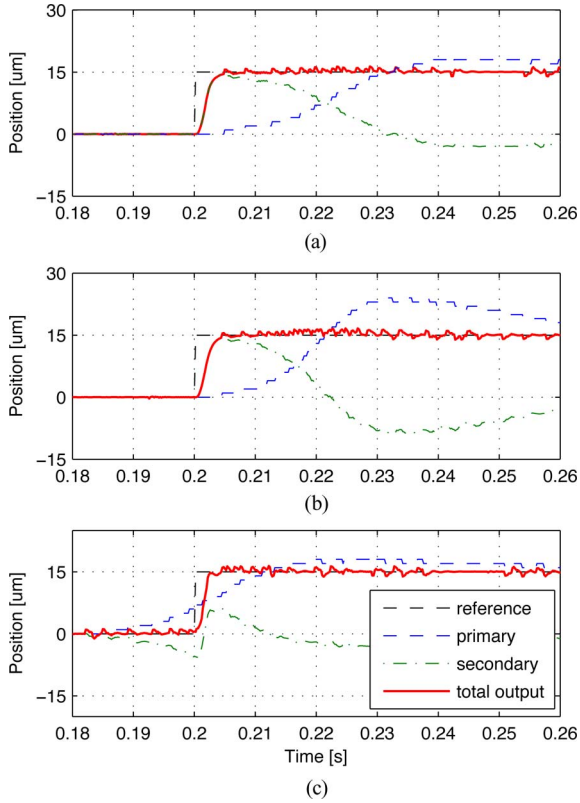

Fig. 4. Dual-stage tracking control for a 15-μm step reference. The proposed control design (c) has a settling time of 2.2 ms and a preview control time of 15.2 ms.

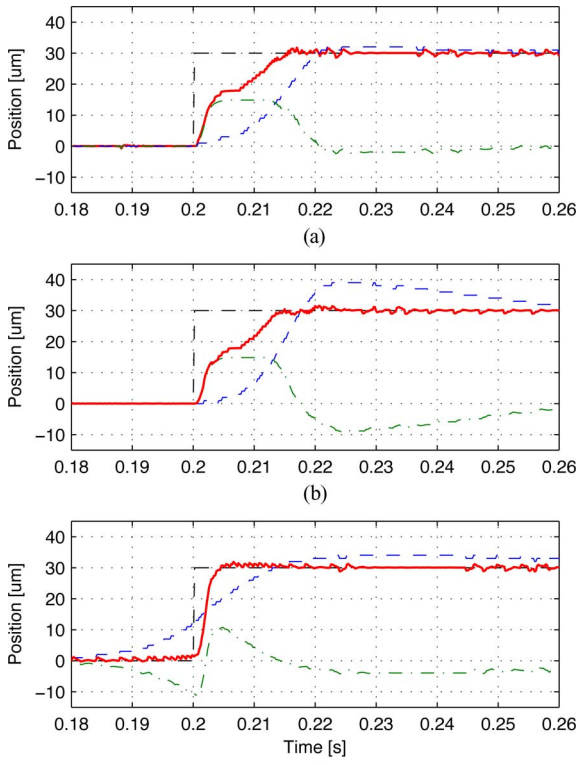

Fig. 5. Dual-stage tracking control for a 30-μm step reference. The proposed control design (c) has a settling time of 3.8 ms and a preview control time of 20.0 ms.

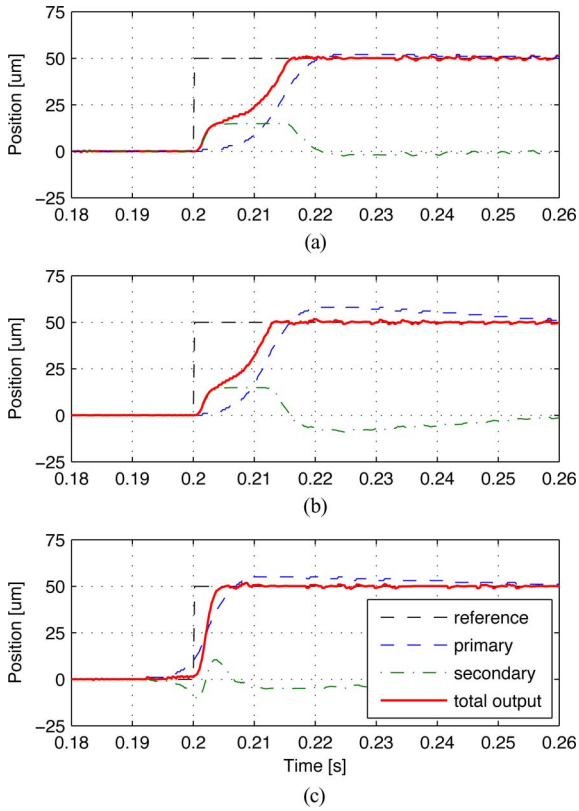

Fig. 6. Dual-stage tracking control for a 50-μm step reference. The proposed control design (c) has a settling time of 4.4 ms and a preview control time of 7.8 ms.

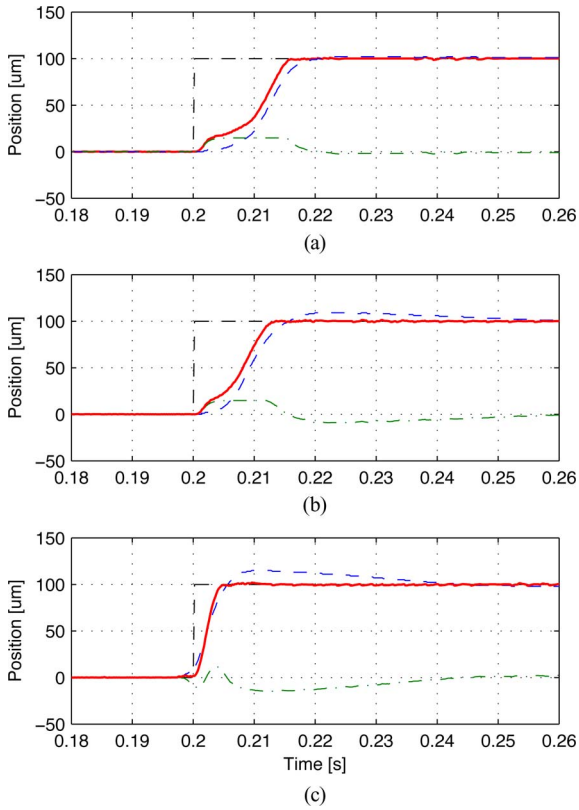

Fig. 7. Dual-stage tracking control for a 100-μm step reference. The proposed control design (c) has a settling time of 4.6 ms and a preview control time of 2.6 ms.

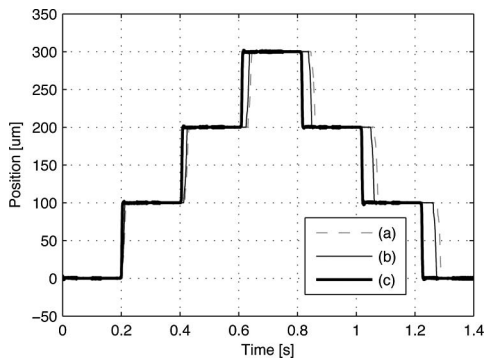

Fig. 8. Staircase response for the three different types of controllers. Here, only the total output y is depicted.

A more significant improvement can be seen in Figs. 5–7, where the references consist of 30, 50, and 100 μm steps. In these cases, the dynamics of the primary actuator play a crucial role in the overall response of the system. Notice, from the plots, that when the secondary actuator saturates the total response suddenly slows down and the system takes a longer time to settle at the reference. This is due to the fact that during the saturation of the secondary actuator, the system can only respond as fast as the primary actuator does. Analyzing these plots, one can clearly see the contribution of the proposed design by noticing that the secondary actuator does not saturate in any of these responses. This fact results in a significant reduction of the settling time because the system is not dominated by the dynamics of the primary actuator.

TABLE I
COMPARISON OF THE SETTLING TIME IMPROVEMENT

Travel Distance (μm)	Improvement ratio achieved by the proposed preview control strategy (%)		
	Single Stage	Controller (a)	Controller (b)
15	92.1	29.0	31.3
30	80.0	73.8	70.7
50	79.4	74.0	68.3
100	76.6	71.6	65.4

Fig. 8 depicts the successive setpoint scenario, where the system follows a staircase reference of 100, 200, and 300 μm. It was assumed that the total output y should stay at each reference for $t_S = 200$ ms. As in the preview plots, the CNF controller is represented by (a), the overshooting controller without preactuation is represented by (b), and the proposed control law is depicted by (c). A comparison between the three controllers is summarized in Table I.

These plots demonstrate the effectiveness of the proposed design. With the knowledge of the time to be spent in each reference (t_S) and the information of immediate future reference levels (ref_2), a significant improvement on the reduction of the transition time is achieved by the proposed preview control strategy.

V. CONCLUSION

A form of preview control for DSA systems was presented in this paper. Based on the information of future reference levels, a control strategy was developed so that inputs were applied before the output transition time interval. This control strategy was carefully designed to take full advantage of the redundancy of actuators and enable them to move, while maintaining the total output at a constant value. Experimental results showed the effectiveness of the proposed approach, which is able to significantly reduce the output transition time of the overall DSA system.

REFERENCES

[1] M. Workman, "Adaptive proximate time-optimal control servomechanisms," Ph.D. dissertation, Stanford Univ., Stanford, CA, 1987.

[2] Z. Lin, M. Pachter, and S. Banda, "Toward improvement of tracking performance-nonlinear feedback for linear systems," *Int. J. Control*, vol. 70, pp. 1–11, 1998.

[3] K. Peng, B. M. Chen, T. H. Lee, and V. Venkataramanan, "Design and implementation of a dual-stage actuated HDD servo system via composite nonlinear control approach," *Mechatronics*, vol. 14, pp. 965–988, 2004.

[4] G. Herrmann, B. Hredzak, M. C. Turner, I. Postlethwaite, and G. Guo, "Discrete robust anti-windup to improve a novel dual-stage large-span track-seek/following method," *IEEE Trans. Control Syst. Technol.*, vol. 16, no. 6, pp. 1342–1351, Nov. 2008.

[5] J. Zheng and M. Fu, "Nonlinear feedback control of a dual-stage actuator system for reduced settling time," *IEEE Trans. Control Syst. Technol.*, vol. 16, no. 4, pp. 717–725, Jul. 2008.

[6] D. Iamratanakul, B. Jordan, K. K. Leang, and S. Devasia, "Optimal output transitions for dual-stage systems," *IEEE Trans. Control Syst. Technol.*, vol. 16, no. 5, pp. 869–881, Sep. 2008.

[7] D. Iamratanakul and S. Devasia, "Minimum-time/energy, output transitions for dual-stage systems," *Trans. ASME, J. Dyn. Syst., Meas., Control*, vol. 131, pp. 1–8, Mar. 2009.

[8] K. W. Chan, W. H. Liao, and I. Y. Shen, "Precision positioning of hard disk drives using piezoelectric actuators with passive damping," *IEEE/ASME Trans. Mechatronics*, vol. 13, no. 1, pp. 147–151, Feb. 2008.

[9] J. Zheng, M. Fu, Y. Wang, and C. Du, "Nonlinear tracking control for a hard disk drive dual-stage actuator system," *IEEE/ASME Trans. Mechatronics*, vol. 13, no. 5, pp. 510–518, Oct. 2008.

[10] J. Zheng, W. Su, and M. Fu, "Dual-stage actuator control design using a doubly coprime factorization approach," *IEEE/ASME Trans. Mechatronics*, vol. 15, no. 3, pp. 339–348, Jun. 2010.

[11] L. Mostefai, M. Denaï, and Y. Hori (2009, Nov. 13). "Robust tracking controller design with uncertain friction compensation based on a local modeling approach," *IEEE/ASME Trans. Mechatronics (99)*, pp. 1–11 [Online]. Available: http://ieeexplore.ieee.org, DOI: 10.1109/TMECH.2009.2033315.

[12] J. Yi, S. Chang, and Y. Shen, "Disturbance-observer-based hysteresis compensation for piezoelectric actuators," *IEEE/ASME Trans. Mechatronics*, vol. 14, no. 4, pp. 456–464, Aug. 2009.

[13] G. F. Franklin, J. D. Powell, and A. Emami-Naeini, *Feedback Control of Dynamic Systems*, 3rd ed. Reading, MA: Addison-Wesley, 1994.

[14] B. Hredzak, G. Herrmann, and G. Guo, "A proximate-time-optimal control design and its application to a hard disk drive dual-stage actuator system," *IEEE Trans. Magn.*, vol. 42, no. 6, pp. 1708–1715, Jun. 2006.

[15] B. M. Chen, T. H. Lee, K. Peng, and V. Venkataramanan, *Hard Disk Drive Servo Systems*, 2nd ed. Secaucus, NJ: Springer-Verlag, 2006.

A Balancing Control Strategy for a One-Wheel Pendulum Robot Based on Dynamic Model Decomposition: Simulations and Experiments

Hongzhe Jin, Jongmyung Hwang, and Jangmyung Lee

***Abstract*—A dynamics-based posture-balancing control strategy for a new one-wheel pendulum robot (OWPR) is proposed and verified. The OWPR model includes a rolling wheel, a robot body with a steering axis, and a pendulum for lateral balancing. In constructing the dynamic model, three elements are generalized in comparison with existing robotic systems: the mass and inertia of the robot body, the "I"-type pendulum, and the steering motion. The dynamics of the robot are derived using a Lagrangian formulation to represent the torques of the wheel during the rolling, yawing, and pitching of the robot body, in terms of the control inputs. The OWPR dynamics are decomposed into state-space models for lateral balancing and steering, and the corresponding controller is designed to be adaptive to changes in the state variables. Simulations and experimental studies are presented that demonstrate and verify the efficiency of the proposed models and the control algorithm.**

***Index Terms*—Gain scheduling, one-wheel pendulum robot (OWPR), posture balancing, speed control.**

I. INTRODUCTION

In the field of constructive nonlinear control, the stabilization problem for unstable nonlinear dynamic systems has been intensively studied [1]–[5]. From pedagogical and theoretical standpoints, the one-wheel robot (OWR) is an excellent model to evaluate an advanced control design, since it is a typically unstable system. Thus far, posture-balancing control problems for OWRs with both horizontal and vertical rotors and a gyroscope have been investigated in terms of various aspects [6]–[8]. The common approach is that the lateral posture is stabilized indirectly by the reaction forces from the motion

Manuscript received March 12, 2009; revised July 8, 2009, November 21, 2009, January 30, 2010, and March 30, 2010; accepted June 12, 2010. Date of publication July 23, 2010; date of current version May 11, 2011. Recommended by Technical Editor Y. Li. This work was supported by the Korea Science and Engineering Foundation, Korea Government (Ministry of Education, Science, and Technology) under Grant R01-2007-000-10171-0.

The authors are with the Department of Electronics Engineering, Pusan National University, Busan 609-735, Korea (e-mail: jmlee@pusan.ac.kr).

Digital Object Identifier 10.1109/TMECH.2010.2054102